NON-UNIFORM 3D DISTANCE TRANSFORM FOR ANISOTROPIC SIGNAL CORRECTION IN CONFOCAL IMAGE VOLUMES OF SKELETAL MUSCLE CELL NUCLEI

Patrick Karlsson Edlund

Centre for Image Analysis
Uppsala University
Sweden

Joakim Lindblad

Centre for Image Analysis
Swedish University of Agricultural Sciences
Sweden

ABSTRACT

Detailed description of the three dimensional organization of nuclei in confocal microscope image volumes of skeletal muscle fibers needs accurate identification of the nuclei centroids. We propose a model based method, applied as a weighted distance transform that take into consideration the diffuse, attenuated, anisotropic, and non-symmetric behavior of the nuclei signals, to provide a transformed image volume where the individual nuclei are better separated, and where the correct nuclei centroids are easily attained.

Index Terms— Image processing, Morphological operations, Microscopy, Biological cells, Muscles

1. INTRODUCTION

Current research of skeletal muscle fibers include analysis of 3D volume images, instead of 2D slices [1, 2]. To describe the organization of nuclei within a volume image of a muscle fiber, a decisive approach for extraction of the nuclei centroids is necessary. The aim of this work is to provide the means for simple identification of the centroids of nuclei within single skeletal muscle fibers. A recurring problem in confocal microscope volume images is anisotropic stray signals, which lead to under-segmentation of weak or closely positioned signals. The intensities of the diffuse nuclei signals are also dependent on the amount of tissue that occludes the nuclei.

A slice of an image volume containing a single muscle fiber is seen in Fig. 1(a), where the fiber cross-section (XZ-plane) along the Y-axis has an elliptical shape. A fiber contain several nuclei, which are not generally spherical objects, but rather elongated disc shaped objects that may be thought of as discs *lying* on a the surface of an elliptical cylinder. We want to separate individual nuclei in the stack of confocal microscope images. However, a captured signal from a nucleus does not show its shape clearly in three dimensions due to several reasons. Due to the shape of the point spread function the distance between two imaging planes in a Z-stack of confocal images is generally larger than the distance between two image elements within an image plane. The sampling density is limited by a number of factors, such as the thickness of the specimen being imaged; bleaching of the fluorescent stain due to prolonged exposure to an exciting laser, computer memory limitations, and time limitations for the operator. The acquired anisotropic signal from a nucleus is not centered around the centroid of the *true* nucleus, but is shifted toward the objective lens. A large part of the acquired signal is made up of a stray diffuse signal that elongate the *true* nucleus signal along the focal axis (Z-axis) well outside the con-

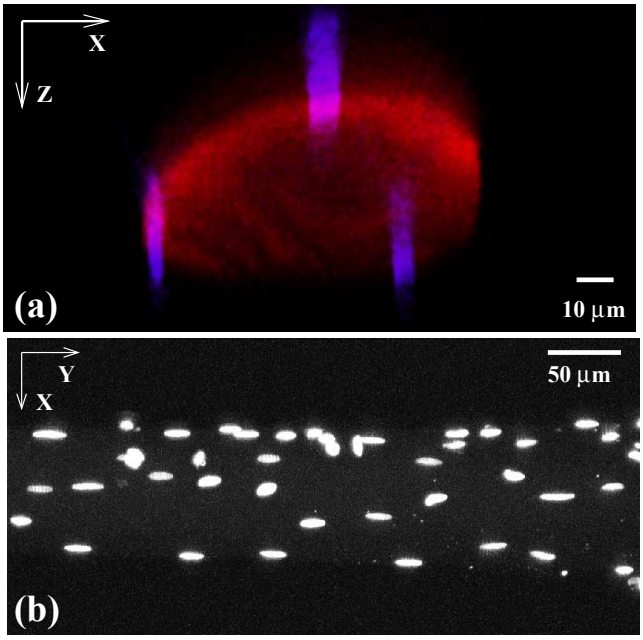

Fig. 1. (a): A slice through a confocal microscope Z-stack showing sarcomeric actin of a fiber (red), and nuclei (blue). (b): A maximum intensity projection (MIP) of a confocal microscope image stack showing all nuclei signals.

We thank the Swedish Science Council for economic support, and Dr. Anna-Stina Höglund and Prof. Lars Larsson at the Department of Clinical Neurophysiology, Uppsala University, Sweden, for scientific support.

The underlying study providing the skeletal muscle tissue for this study was approved by the Ethical Committee on Human Research at Uppsala University, Uppsala, Karolinska Institute, Stockholm, Sweden, and by the Institutional Review Board at Pennsylvania State University, USA.

fines of the *true* nucleus border. If two nuclei are positioned close to each other along the Z-axis the signals interact with each other making identification of the individual nuclei difficult. Due to tissue opacity the captured signal from the inside of a specimen is attenuated. Thus, the signal from a nucleus has lower intensity if it is occluded by fiber tissue. In this sense, a single nucleus is also occluding itself, and the signal intensity of the nucleus part closer to the objective lens is stronger than the intensity in the part of the nucleus that is further away from the objective lens. The varied non-spherical shapes and positioning of the imaged nuclei, affected by attenuation and a large anisotropic effect, require an elaborate method for identifying the individual nuclei centroids.

We propose a method based on distance transformation to separate diffuse nuclei signals, applied anisotropically to compensate for stray signals along the Z-axis, supported by attenuation correction for signals occluded by tissue, and using gray levels in the distance transform for robustness against noise. To our knowledge, no similar approach, using a spatially modulated distance transform, has been presented earlier.

2. IMAGE ACQUISITION

Single permeabilized skeletal muscle fibers are attached to a 3D manipulator (Uppsala University, Uppsala, Sweden) exposing 1 mm, or more, of the fiber in a relax solution [3]. Volume images are acquired using a Zeiss laser scanning confocal microscope, LSM 510 Meta (Carl Zeiss, Germany), fitted with a Plan-Neofluar 20x/0.5 lens. The tissue samples were stained by 4,6-diamino-2-phenylindole (DAPI) excited by laser line 405 nm, and detected through BP filter 420–480 nm. For fiber volume actin was labeled by rhodamin-phalloidin excited by laser line 543 nm, and detected through a BP filter 560–615 nm. The image elements (non-cubic voxels) are of size $0.45 \times 0.45 \times 0.90 \mu m^3$. To create cubic voxels, each original image element is cut in half along the Z-axis, which gives two cubic voxels with an individual volume of $0.45 \times 0.45 \times 0.45 \mu m^3$. A typical volume contain approximately $500 \times 1000 \times 100$ non-cubic voxels with a total volume of $225 \times 450 \times 90 \mu m^3$.

3. METHOD

The proposed method for identifying nuclei centroids use different approaches to address the issues involved in separating the diffuse nuclei signals, correcting for the signal attenuation, and transforming the anisotropic stray signals around the nuclei signals. A distance transform (Sec. 3.1) is used as the underlying method, and is subsequently altered by an attenuation correction (Sec. 3.3) that estimates the tissue thickness above a given signal (Sec. 3.2), a procedure that introduce anisotropic scaling in the distance transform (Sec. 3.4), and a procedure that uses the underlying gray levels in the volume image to enhance the robustness to image noise (Sec. 3.1). The method output is a volume with distance values assigned to the image elements instead of signal intensities (Sec. 3.5).

3.1. Distance transform

A distance transform (DT) calculates the smallest distance between an object voxel, and the nearest background voxel. A framework for the chamfer distance transform applied to binary images was presented in [4], and further developed in [5]. A gray level weighted distance transform (WDT) was presented in [6]. The WDT take the underlying gray levels into consideration when assigning a distance value to an object voxel. A weak intensity implies a shorter distance to the background for a specific voxel, compared to the same voxel having a stronger intensity. The Chamfer(3,4,5) DT [4] was selected as the basic DT for the method, due to its speed, simple implementation, and low error [5]. The formula for calculating the WDT chamfer weight g_i for the a $3 \times 3 \times 3$ mask centered at p is

$$g_i = \frac{1}{2}(I_p + I_i)\, w_i \,, \tag{1}$$

where I is the intensity of the image voxel at position i or p, and $w \in \{3, 4, 5\}$. The range of the intensity in the image volume is assumed to be $[0, 1]$. The Chamfer(3,4,5) DT can be performed in one *forward*, and one *backward* pass, while a typical WDT requires $3 - 4$ forward, and backward passes before distances converge. This behavior is due to the propagation of distance values along non-straight paths.

3.2. Tissue thickness

We assume that the tissue occluding the nuclei signals has an elliptical cross-section centered at the center of an images slice as shown in Fig. 2(a). The thickness of the tissue occluding a nuclei at depth z is

$$h(z) = \begin{cases} 0 & \text{if} \quad z \leq H/2 \\ 2z - H & \text{if} \quad z > H/2, \end{cases} \tag{2}$$

where H is the height (or depth) of the Z-stack. The modeled tissue thickness is correct assuming that the nuclei only appear on the outer perimeter of the elliptical cross-section.

3.3. Attenuation correction

An equation that describe the signal attenuation in fluorescence microscopy is given by [7] to be

$$I_\lambda(z) = I_0 e^{-\alpha z} \,, \tag{3}$$

where $I_\lambda(z)$ is the collected light at wavelength λ, depending on the focal position z. I_0 is the underlying intensity, and the attenuation coefficient α is the sum of the attenuation coefficients for the exciting α_{ex}, and emitted light α_{em}. The

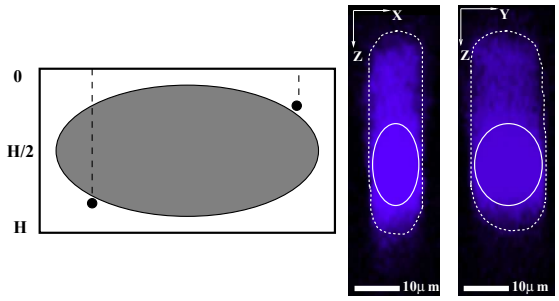

(a) Tissue model. (b) XZ. (c) YZ.

Fig. 2. (a): The amount of tissue occluding a nucleus at $z > H/2$ is estimated to be twice the Z-distance between the nucleus and $H/2$, where H is the height of the Z-stack. (b)–(c): 2D slices through the center of a nucleus (along the focal axis) of a non-isotropic signal. The bulk of the stray signal is in the Z-dimension. The amount of stray signal is less below the nucleus.

attenuation coefficients are different due to the respective differences between excitation and emission wavelengths. The attenuation coefficient α represent the combined effect of absorption, scattering, and refraction. For more details on calculations see the Appendix in [8]. The value of the attenuation coefficient α is selected as

$$\alpha = \ln(1+b)/H\,, \tag{4}$$

where H is the height of the Z-stack, and b is a parameter in $[0, 1]$ that sets the maximum level of the attenuation correction, i.e., $1 + b$ is the maximum value of $1/e^{-\alpha z}$ at $z = H$.

3.4. Anisotropic signal correction

The signal from a nucleus is not isotropic, see Fig. 2(b), and 2(c). The contrast between signal and background is high in the XY-plane, but low along the Z-axis. This stray signal is not symmetric around the *true* nucleus, but is more noticeable above the *true* nucleus (i.e., closer to the exciting laser), and less below the *true* nucleus. This stray signal is exhibited by all nuclei signals, also if the nucleus has occluding tissue between itself and the exciting laser. We compensate for the anisotropy by applying a position dependent scaling of the local distances in the WDT. The scaling of the WDT is only applied to elements in the chamfer mask that are above, or below the currently investigated voxel p (at focus plane z). The distance weights above p, i.e., at focus plane $z - 1$, are scaled down with a number $d \in [0, 1]$. The distance weights of elements below p, i.e., at focus plane $z + 1$ are also scaled down, but with a new d that is greater than the d at $z - 1$, but still in $[0, 1]$. The difference Δd between $d(z - 1)$, and $d(z + 1)$ is kept constant for all z. The values of $d(z \pm 1)$ are selected to be lower for low z, i.e., closer to the objective lens, than for focus planes further away from the lens. The two behaviors above are modeled by

$$d(z) = \frac{a_2 - a_1}{H}\, z + a_1\,, \tag{5}$$

where $d(z)$ is a straight line between $a_1 \in [0, 1]$, and $a_2 \in [0, 1]$, and $a_1 < a_2$. The difference Δd is $2(a_2 - a_1)/H$.

3.5. Complete transform

The proposed mask element weights for the distance transformation, using Eq. 1, 2, 3, and 5 are thus

$$g_i = \frac{1}{2}(I_p/e^{-\alpha h(z)} + I_i/e^{-\alpha h(z\pm1)})\, w_i\, d(z \pm 1)\,, \tag{6}$$

when i is at $z \pm 1$, and where p is at focus plane z, and α is chosen as described by Eq. 4, and

$$g_i = \frac{1}{2}(I_p + I_i)/e^{-\alpha h(z)}\, w_i\,, \tag{7}$$

when i is at focus plane z. The coordinates x, and y are not shown in Eq. 6, and 7.

4. APPLICATION

A fiber volume (see Sec. 2) is subdivided into sub-volumes to lower the computational cost. A maximum intensity projection (MIP) of the image volume along the focal axis (i.e., the Z-axis perpendicular to the XY imaging plane) reveal areas in which nuclei are present, see Fig. 1(b). Sub-volumes are extracted from the Z-stack based on the corresponding MIP, which is clustered into background and nuclei signal using fuzzy c-means clustering [9]. The resulting 2D nuclei signal clusters define 3D bounding boxes, such that the sub-volumes contain one or more nuclei, since signals may be connected, or occluding each other in part or in whole along the Z-axis. A typical sub-volume contains approximately $20 \times 40 \times 200$ cubic voxels with a total volume of $9 \times 18 \times 90 \mu m^3$. The proposed method is applied to the sub-volumes one at a time. The output volumes have the same sizes as the input sub-volumes, and the values within each image element is the shortest distance to the background (see Sec. 3.5). The MIP in Fig. 3, and 4 ($b = 0.1$, and $[a_1, a_2] = [0.1,\ 1.0]$) illustrate how the proposed method transform the input sub-volumes into new sub-volumes that better represent the imaged data, with respect to the number of nuclei, and centroid position.

5. DISCUSSION

The proposed method corrects the acquired skeletal muscle nuclei signals from confocal microscope Z-stacks, so that the *true* nuclei centroids are extracted where expected. This is achieved by applying an spatially modulated distance transform to the anisotropic nuclei signals. By treating the nuclei signals differently depending on their position within

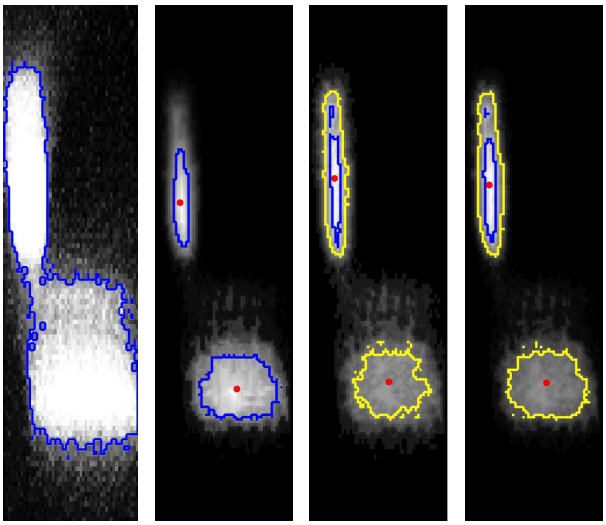

(a) MIP (b) Method (c) DT (d) WDT

Fig. 3. (a): MIP of a sub-volume with two similar disc-shaped nuclei, one rotated 90° in relation to the other. The blue curve represent the border between background and foreground as calculated by fuzzy c-means clustering. (b): A MIP of the result from applying the proposed method on the same sub-volume. The blue iso-surface curves provide borders between relevant parts of the true nuclei signals, and the rest of the volume. Note the position of the centroids. (c): MIP of a standard DT. The blue border represent the threshold that give the signal at the top of the volume similar area properties as in image (b). Note the shift of centroids, and that the threshold excludes the signal at the bottom of the image. The yellow border represent the threshold that gives the nuclei signal at the bottom the same area properties as in image (b). (d): MIP of a WDT, where the dark and bright borders are positioned according to the same principles as in (c).

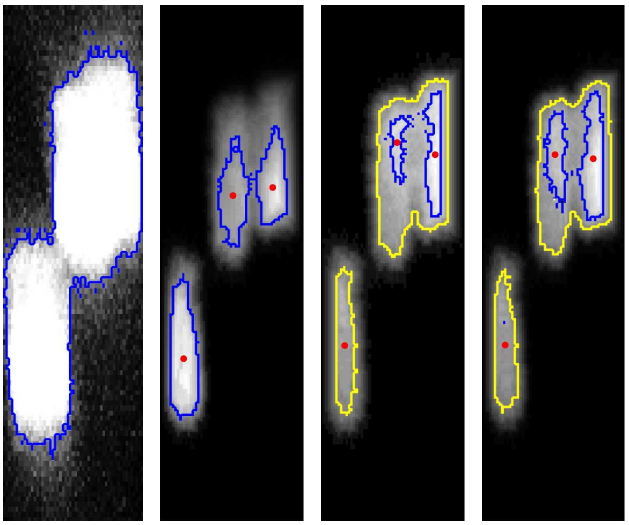

(a) MIP (b) Method (c) DT (d) WDT

Fig. 4. (a): A MIP of three nuclei where two nuclei are very close to each other. (b): The method separates the signals (blue) when no good threshold can be found for standard DT or WDT ((c) and (d)). Notice the shift of centroids.

the image, and transform them differently along the Z-axis, than along the X-, and Y-axis automatic centroid extraction is greatly simplified. The parameter selection is done once before applying the method to a large set of image volumes acquired with the same settings on the confocal microscope. The method is applied in current research projects dealing with organizational differences between different species, such as mouse, rat, human, pig, horse, and rhinoceros, and also for characterizing 3D muscle fiber changes in humans due to aging. Future work include adapting the method for challenging work regarding characterizing the 3D organization in deceased, and abnormal skeletal muscle fibers, where nuclei often are highly clustered.

6. REFERENCES

[1] J. C. Bruusgaard et al., "Number and spatial distribution of nuclei in the muscle fibres of normal mice studied in vivo," *J Physiol*, vol. 551, no. 2, pp. 467–478, 2003.

[2] J. C. Bruusgaard et al., "Distribution of myonuclei and microtubules in live muscle fibers of young, middle-aged, and old mice," *J Appl Physiol*, vol. 100, pp. 2024–2030, 2006.

[3] L. Larsson et al., "Maximum velocity of shortening in relation to myosin isoform composition in single fibres from human skeletal muscles," *J Physiol*, vol. 472, no. 1, pp. 595–614, 1993.

[4] G. Borgefors, "Distance transformations in arbitrary dimensions," *CVGIP*, vol. 27, pp. 321–345, 1984.

[5] B. J.H. Verwer, "Local distances for distance transformations in two and three dimensions," *Pat Rec Let*, vol. 12, pp. 671–682, 1991.

[6] D. Rutovitz, "Data structures for operations on digital images," in *Pictorial Pattern Recognition*, Washington D.C., 1968, pp. 105–133, Thompson Book Company.

[7] S. T. Flock et al., "Optical properties of intralipid: A phantom medium for light propagation studies," *Lasers Surg Med*, vol. 12, no. 5, pp. 510–519, 1992.

[8] A. Can et al., "Attenuation correction in confocal laser microscopes: a novel two-view approach," *J Microsc*, vol. 211, no. 1, pp. 67–79, 2003.

[9] J. C. Bezdek, *Pattern Recognition with Fuzzy Objective Function Algorithms*, Kluwer Academic Publishers, Norwell, MA, USA, 1981.